Investigating the Accuracy of Eddy Current Simulation and Evaluation for Rail Testing

Alexander Friedrich *

Bundesanstalt für Materialforschung und -prüfung, Division 8.4 Acoustic and Electromagnetic Methods

October 28, 2024

Abstract

Eddy current testing is a non-destructive evaluation (NDE) technique that is widely used for testing railway rails with a strong focus on detecting cracks. In this paper, we investigate the accuracy of eddy current simulation and eddy current evaluation in the context of rail testing. We focus on analyzing the numerical accuracy of BEM simulations depending on the mesh size relative to the skin depth, and on estimating the influence of simplifying assumptions for cracks. Specifically, we consider the defect width, surface geometry, testing train velocity and material parameter change. We provide relative error estimates and we propose a regime for systematic rail defect simulation.

Keywords: eddy current simulation, eddy current testing, rail testing, non-destructive testing

1 Introduction

In the project Artificial Intelligence for Rail Inspection (AIFRI) we aim to improve the detection and classification accuracy for rail testing data by developing machine learning based evaluation algorithms. Simulation of eddy current signals is crucial for providing synthetic data to train and evaluate the performance of the evaluation algorithm. However, accurate eddy current simulation and eddy current evaluation is challenging due to the complex physics involved.

In [2] Bao et. all. carried out an analysis of the simulation accuracy for eddy current non-destructive testing problems similar to the one of section 3. However, they worked with a different material and probe setup, and did not discuss the simulation accuracy in the presence of defects. Since they only consider the baseline eddy current signal but not the change of the signal in the presence of a defect, we expect to find significantly higher errors in our analysis as the signal amplitude decreases by about one order of magnitude. In [7] Yusa et. al. discuss the simulation of eddy current testing for fatigue cracks with regard to the defect geometry. They conclude that a crack width of 0.2 mm is adequate in the case of austenitic steel. However, they use a different simulation method and do not quantify their result.

Estimating geometric parameters of crack like defects using eddy current test data is widely used in NDE applications, but it also has high inherent uncertainties. In [6], Yusa et. al. show that even using FEM models fitted to specific, high resolution eddy current scans of stress corrosion cracks exhibit an error of 60 % for the estimated depth of the crack. They conjecture that the success in estimating the depth of cracks from previous studies was due to their simplified design. This is perhaps reflected in the paper [4] by Pohl et. al. where they investigate the question of depth estimation in the context of rail testing. They find errors of 5 % to 20 % in their laboratory setup, using a reference block with notches manufactured from a railway rail. Furthermore, they discuss other factors that can influence the accuracy. In particular, they estimate that the uncertainty of the interior angle of real cracks contributes a 20 % error. The study of Pohl et. al. was carried out

*Alexander.Friedrich@bam.de

in our laboratory and we repeated the testing of the reference block in the course of the AIFRI project. We are able to interpolate the relation of the eddy current signal and the depth of notches. Thus we can calculate the error of the eddy current signal, given an error of the depth. In the depth range of 0.5 mm to 2.0 mm, which we discuss in this article, the signal error is approximately the same as the depth error; i.e. the modulus of continuity is approximately the identity. Thus we have a 5 % to 10 % signal error in the laboratory test data.

In this article we pursue a twofold goal. For one we directly estimate the simulation accuracy depending on the mesh size measured in terms of the skin depth in the rail testing setting. Secondly, we quantify the influence of simplifying assumptions made in the evaluation of eddy current rail test data by systematic simulations. Finally, we may combine these results to determine an effective accuracy for simulated, synthetic eddy current test data. The data used for the present article is available for download, see [3].

2 Methodology

2.1 Model Design and Parameter Settings

In order to recreate the railway rail testing setup we developed a simplified model of the HC10 eddy current probe employed on testing trains operated in Germany, see figure 1. We used an eddy current reference block to fit and validate our model parameters. For the rail steel we found $\mu_r = 41$, and $\sigma = 2.16\,\mathrm{MS\,m^{-1}}$. The HC10 probe consists of an inner, and an outer ferrite core as well as a steel frame. We fitted the following material parameters: $\mu_{r,\,core,\,inner} = 300$, $\mu_{r,\,core,\,outer} = 300$, $\mu_{r,\,frame} = 363$, $\sigma_{frame} = 1.84\,\mathrm{MS\,m^{-1}}$. The probe is operated at a frequency of 150 kHz.

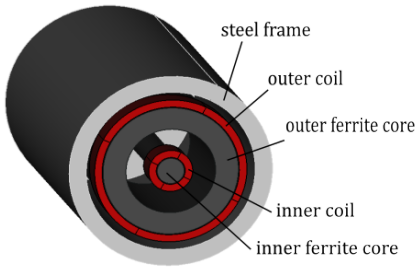

Figure 1: CAD model of the simplified HC10 probe

We carried out the simulation on a desktop computer with an Intel Xenon Silber 4108 CPU, 8 cores, 1.8 GHz, and 240 GiB RAM; using the Faraday software [5] and its BEM solver.

In section 3 we evaluate the signal at a point directly above a defect. In 4 we consider the signal along a line orthogonal to the notch. In any case, the signal for a defect is a complex voltage and is obtained by subtracting the corresponding baseline signal without the presence of a defect. Additionally, the testing system is calibrated such that the probe liftoff signal mostly effects the real part of the signal. To that end, the test and simulation signal are shifted by $(1.35 + 3.09\mathrm{i})\,\mathrm{V}$ and rotated by $-2.84\,\mathrm{rad}$.

2.2 Simulation Accuracy and Mesh Size

To analyze the accuracy in relation to the mesh size we proceed similarly as Bao et. all in [2], that is we choose the skin depth of the test specimen as reference scale. Let δ be the skin depth of the test specimen. For the fitted rail steel we have $\delta = 0.14\,\mathrm{mm}$. Let Σ be a part of the surface of the specimen. For N the number of cells in Σ define the characteristic mesh size of Σ as $\lambda := \sqrt{\frac{|\Sigma|}{N\delta^2}}$. In each of the experiments of section 3 we vary λ for different probe and material combinations. We expect the simulation to converge for small λ, and present pointwise error estimates relative to result with the lowest λ.

We carried out simulation experiments using a rectangular cuboid with a square top face and an edge length of 14 mm with a rectangular notch. The probe is placed in the center of the top face, 1.0 mm above the test specimen, mirroring the rail testing setup. The notch is 0.1 mm wide and its depth ranges from 0.5 mm to 2.0 mm in 0.5 mm steps. The depth of the cuboid is adapted, such that it is always 2.0 mm larger then the depth of the notch.

2.3 Simplifying Assumptions and Test Conditions

Test data is often evaluated by comparing it against data gathered from a reference block in a laboratory setup. For rail testing this specimen is a rail head with a flatted top and several straight, rectangular, relatively wide notches (0.14 mm to 0.27 mm). Thus, the crack width and rail geometry is implicitly simplified. At the same time the laboratory test are carried out at very small velocities compared to the testing train. Finally, since only one reference is considered the influence of the material parameters on the signal are also neglected. However, we do not discuss the influence of the crack geometry. We analyze the situation, using simulations with two simple models. For the width, the velocity and material parameters we choose a rectangular cuboid with a length of 28.0 mm, a width of 20.0 mm, a rectangular notch of depth 0.5 mm or 2.0 mm and a width of 0.1 mm. The depth of the cuboid is chosen such that it is 2.0 mm deeper then the notch. To estimate the influence of the rail head profile we note that the gauge corner of a rail is dominated by two radii, a larger and a smaller one. We simulate different curvature situations on cylindrical test bodies of length 28.0 mm of varying radii with a notch of depth 0.5 mm to 2.0 mm. The HC10 probe is placed 1.0 mm above the test specimen and moved across the specimen in 1.0 mm steps, mirroring the rail testing procedure. In symmetrical setups, i.e. for sections 4.1, 4.2, and 4.4, the only half the signal is simulated.

We present mean L^2, and C^0 error estimates relative to the total signal variation; $\operatorname{var}(f) := \sup_{x,\, y\in I} |f(x) - f(y)|$) for a function $f : I \subset \mathbb{R} \to \mathbb{C}$. Suppose s is the signal to be evaluated and s_0 is the reference signal, then we define the errors ϵ_{L^2} and ϵ_{C^0} as follows.

$$\begin{aligned} \epsilon_{L^2}(s) &:= \frac{\|s - s_0\|_{L^2}}{|\operatorname{supp}(s - s_0)|\operatorname{var}(s_0)} \\ \epsilon_{C^0}(s) &:= \frac{\|s - s_0\|_{C^0}}{\operatorname{var}(s_0)} \end{aligned}$$

Here supp is the support of a function, i.e. the set where it is non zero. While the C^0 error can be thought of as the difference of the peak values of the signal, the L^2 error describes the entire signal shape. With the above convention the L^2 error is always smaller then or equal to the C^0 error. A large L^2 error is indicative that the signal as a whole is not well approximated. Whereas a small L^2 error combined with a rather large C^0 error means that only very few points of the signal deviate from the reference. Of course, the signals we obtain are discrete. Hence, the L^2 error can also be though of as an average of the pointwise error over the support of the signal:

$$\epsilon_{L^2}(s) = \frac{\left(\sum_{i\in I} |s(i) - s_0(i)|^2\right)^{1/2}}{|I|}$$

supposing that s is supported on the discrete set I.

3 Simulation Accuracy Analysis

Due to computation resource constrains we cannot decrease λ beyond 0.6 for our rail testing setup, see figure 2. To remedy this situation we carry out the same analysis for two related cases. First, we keep the complex HC10 probe design, but reduce the permeability and conductivity of the steel. For $\mu_r = 10$ and $\sigma = 1\,\mathrm{MS\,m^{-1}}$ we obtain $\delta = 0.41$ mm. See figure 3a for the results. Secondly, we use the fitted rail steel parameters but replace the probe with a small and simple one - a single coil with 10 mm diameter. See figure 3b for the results. In either case we may reduce λ to 0.2.

We observe a similar monotone increasing behavior for all setups and depths. For the simplified cases we have an error in the low percent points up to $\lambda = 0.6$. For λ larger then 1 we have errors

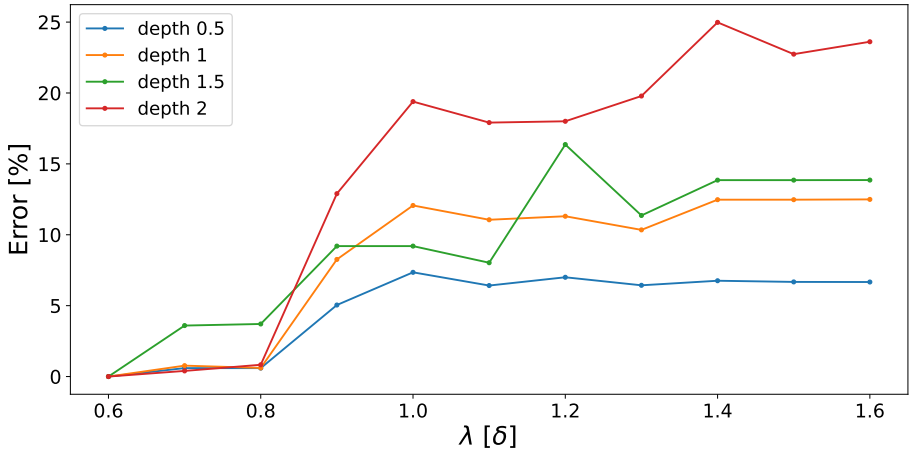

Figure 2: Simulation accuracy; errors for depth d and reference mesh size 0.6

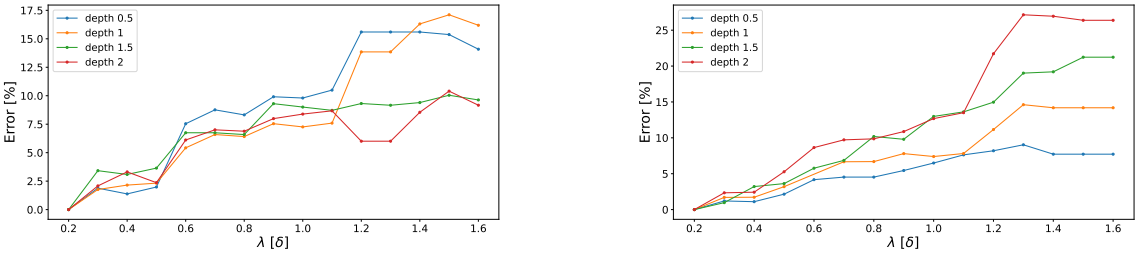

(a) Low μ_r and σ (b) Simple probe

Figure 3: Errors for reference mesh size 0.2

of 10 % to 20 % in all setups. In view of these results, the high inherent uncertainty of the eddy current testing, and the computational constraints we compromise on a mesh size $\lambda = 1.4$ for the simulation experiments of section 4.

4 Influence of Simplifying Assumptions

4.1 Defect Width

We investigate the influence of the crack width on the signal, using a width of 0.1 mm as a reference. We do not decrease the width below 0.1 mm since we would severely undercut the mesh size of $\lambda\delta \approx 0.2$ mm.

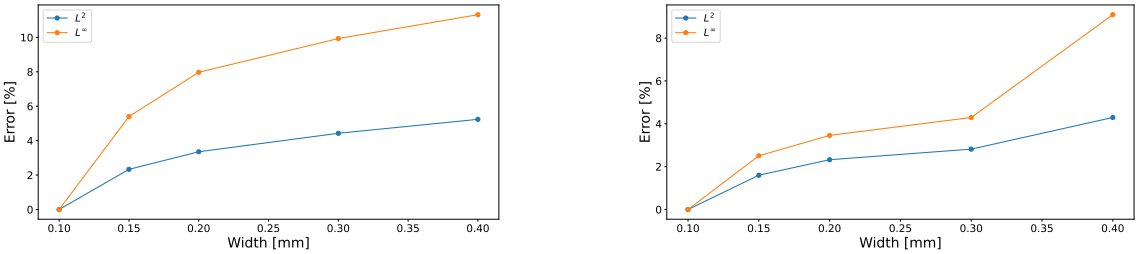

(a) $d = 2.0$ mm (b) $d = 0.5$ mm

Figure 4: Width error estimates for depth d and reference width of 0.1 mm

In figure 4 we clearly see a monotone increasing behavior of both errors and in both cases as the crack width increases. The test block available to us has notches with width from 0.14 mm to

0.27 mm. This corresponds to errors from 5 % to 11 %.

4.2 Surface Curvature

We simulate different curvature situations on cylindrical test bodies. First we analyze the differences between rail head designs. We choose the UIC 60E2 design as a reference, since it is widely used and has generic construction parameters. It has a large radius of 70 mm at the upper gauge corner and a small radius of 16 mm at the lower gauge corner. We investigate a radius range of 60 mm to 400 mm and 12 mm to 17 mm respectively. In this way we cover the upper and lower gauge corner of all rail types documented in the standard [1, Attachment A].

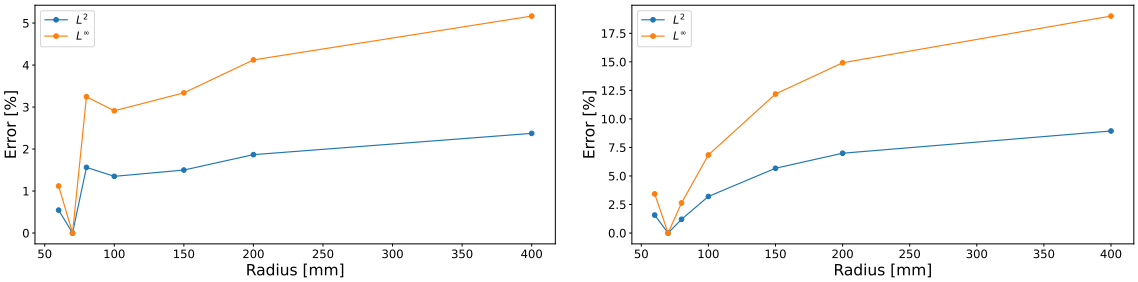

(a) $d = 2.0\,\text{mm}$ (b) $d = 0.5\,\text{mm}$

Figure 5: Radius error estimates for depth d and reference radius 70 mm

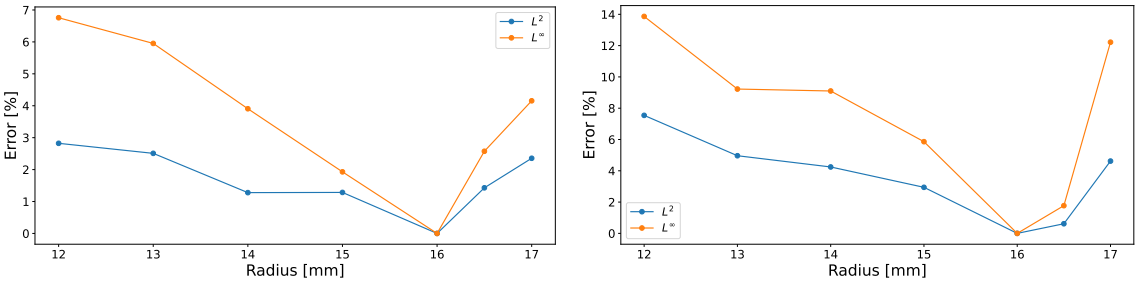

(a) $d = 2.0\,\text{mm}$ (b) $d = 0.5\,\text{mm}$

Figure 6: Radius error estimates for depth d and reference radius 16 mm

Figures 5 and 6 show the errors for the large and small radius respectively. The errors are acceptable, especially if we consider that to our knowledge the UIC rail types 60E2, 49E5 and 54E4 are by far the most commonly used in Germany, and their radii lie within the range of 70 mm to 115 mm and 13 mm to 16.5 mm respectively. In these ranges we have less then 10 % error. We also note that here the error is higher for the smaller defect which speaks for a kind of offset effect, opposed the the cases of sections 4.1, 4.3, and 4.4 where the error is more pronounced for the larger defect.

Next we compare the curvature situations above to the flat geometry of the reference block, which would correspond to a radius of ∞ mm. In figure 7 we see that we accrue a significant error if we compare the signals of the curved surface to a flat reference. In particular in the lower part of the gauge corner we have errors of 23 % to 71 %, but also in the in the upper part of the gauge corner we see errors up to 33 %.

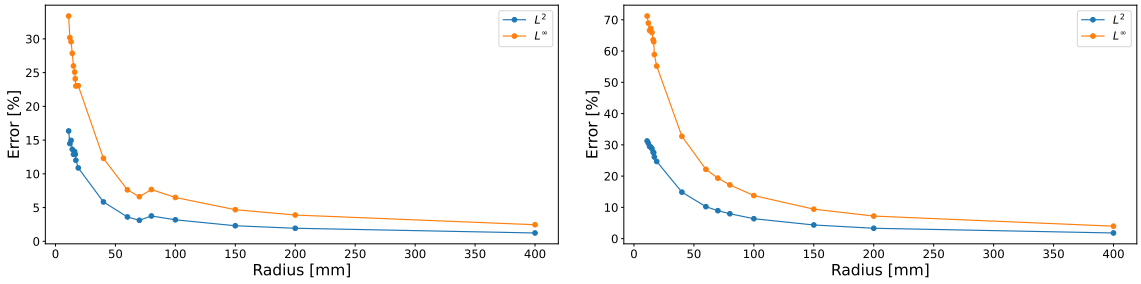

(a) $d = 2.0\,\mathrm{mm}$ (b) $d = 0.5\,\mathrm{mm}$

Figure 7: Radius error estimates for depth d and a flat reference

4.3 Testing Velocity

We investigate the influence of the testing train velocity on the signal and vary the velocity from $5.0\,\mathrm{m\,s^{-1}}$ to $20.0\,\mathrm{m\,s^{-1}}$ in steps of $5.0\,\mathrm{m\,s^{-1}}$. The direction of the velocity is transversal to notches and the reference velocity is $0.0\,\mathrm{m\,s^{-1}}$.

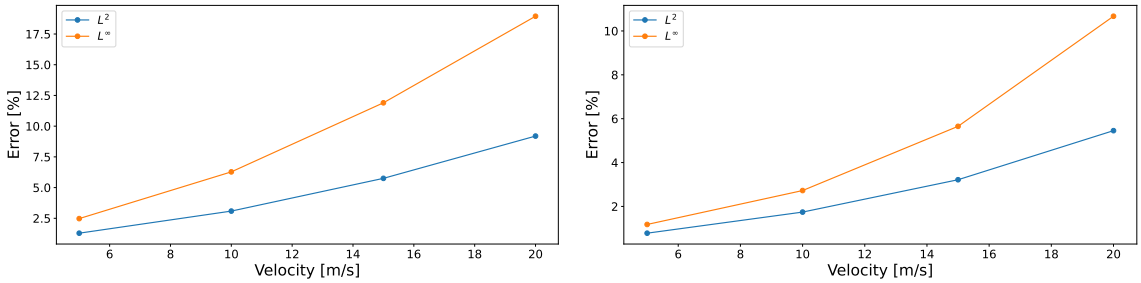

(a) $d = 2.0\,\mathrm{mm}$ (b) $d = 0.5\,\mathrm{mm}$

Figure 8: Errors for depth d and reference velocity $v_0 = 0\,\mathrm{m\,s^{-1}}$

In figure 8 we clearly see a monotone increase in both cases. The testing trains mostly run at velocities of $16.5\,\mathrm{m\,s^{-1}}$ to $20.0\,\mathrm{m\,s^{-1}}$, which corresponds to $60\,\mathrm{km\,h^{-1}}$ to $72\,\mathrm{km\,h^{-1}}$. In this range we find peak errors of 15 % to 19 %. We feel it is necessary to mention that the Faraday guide advises to use their velocity feature with caution since it is rather new. Previous experiments at BAM using a rotationally symmetric reference block with artificial notches clamped in a lathe showed no measurable influence of the eddy current signal on rotation velocity.

4.4 Material Parameter Change

We vary the relative permeability in the range of 30 to 55 and the conductivity in the range of $1.8\,\mathrm{MS\,m^{-1}}$ to $2.4\,\mathrm{MS\,m^{-1}}$. Material parameter changes in this domain can be used to describe welds and effects likely related to hardening of the rail due to rolling contact fatigue. Reference parameters for this analysis are the ones of the fitted rail steel, $\mu_r = 41$, $\sigma = 2.16\,\mathrm{MS\,m^{-1}}$.

In figure 9 we fix conductivity and vary the permeability. In all cases we see a mostly convex behavior with a minor dependence on the conductivity and a stronger dependence on the permeability. Overall the error stays well below 19 %.

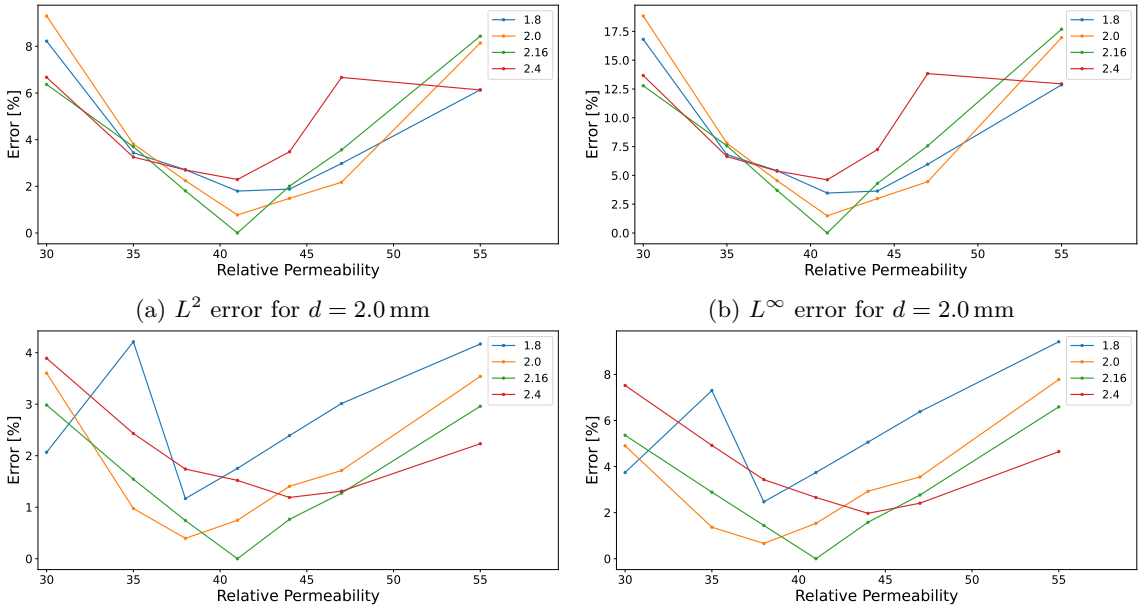

(a) L^2 error for $d = 2.0\,\mathrm{mm}$

(b) L^∞ error for $d = 2.0\,\mathrm{mm}$

(c) L^2 error for $d = 0.5\,\mathrm{mm}$

(d) L^∞ error for $d = 0.5\,\mathrm{mm}$

Figure 9: Material error estimates for depth d

5 Conclusion

Recall that the reference block for rail testing has a flattened surface, 0.14 mm to 0.27 mm wide notches and is tested at very low velocities. If we assume the errors discussed in section 4 are independent we can calculate the total error ranges. In table 1 we display the minimal and maximal C^0 error along with a "likely minimal" error based on the error estimates for the most common values for the velocity ($20.0\,\mathrm{m\,s^{-1}}$) and surface curvature (80 mm), and averages for the material and width.

depth	$\epsilon_{C^0,\,\mathrm{min}}$	$\epsilon_{C^0,\,\mathrm{likely}}$	$\epsilon_{C^0,\,\mathrm{max}}$
0.5 mm	8 %	35 %	96 %
2.0 mm	12 %	43 %	81 %

Table 1: Error estimates of simplifying assumptions, evaluation

These errors are rather large, but comparable to the estimated 20 % from the uncertainty of the internal angle of the defect reported in [4]. Of course, this error needs to be added to the ones listed in table 1 along with any others stemming from the defect geometry, which we did not investigate here.

Note however, that in all cases of section 4 the L^2 error is significantly lower then the C^0 error, often by more then a factor of 2. This means that the signal shape is well approximated, as opposed to the amplitude.

Regarding the accuracy of simulated synthetic data, section 4.2 clearly shows the necessity to use a specific rail head geometry. Any of the widely used UIC models 60E2, 49E5 and 54E4 will result in an error of less then 10 % for the large majority of the rail types. The defect width should be chosen as small as possible while still conforming to the dimension of the mesh size. While the material parameters have no better choice then the reference chosen in 4.4, the velocity should also be chosen as $20\,\mathrm{m\,s^{-1}}$. With this configuration we obtain the error ranges listed in table 2.

However, while using Faraday, we have encountered geometry errors with defects of width 0.1 mm in rail models. Additionally, Faraday states in their guide that the feature of adding velocity to the model is new and should be used with caution. Thus, if we use a width of 0.2 mm and a velocity of $0\,\mathrm{m\,s^{-1}}$ instead, we obtain the following estimates.

depth	$\epsilon_{C^0,\,\mathrm{min}}$	$\epsilon_{C^0,\,\mathrm{max}}$
0.5 mm	0 %	24 %
2.0 mm	0 %	32 %

Table 2: Error estimates of simplifying assumptions, simulation, optimized configuration

depth	$\mathrm{error}_{C^0,\,\mathrm{min}}$	$\mathrm{error}_{C^0,\,\mathrm{max}}$
0.5 mm	5 %	33 %
2.0 mm	11 %	50 %

Table 3: Error estimates of simplifying assumptions, simulation

In either case the error estimates of 5 % to 25 % from section 3 need to be added to the results of the tables 2 and 3.

If we are looking to minimize the error, choosing a mesh size of $1\,\delta$ or $0.5\,\delta$ would be an obvious choice, given the computational resources. Improving the errors induced by the curvature and the material parameters is more challenging. Our curvature analysis is really a stand in for the rail surface geometry. This geometry is more complex then the cylinder models here, especially for used, deformed rails. If we focus just on nominal rail geometry, additionally simulating any of the UIC designs 50E5, 49E2, 46E4, 52E1 with small and large radii in ranges of 12 mm to 14 mm and 350 mm to 400 mm would improve the error estimates. But it should be checked how widely these designs are used. Improving the error due to the material parameter would likely entail adding the permeability as a parameter for the systematic defect simulation. However, this is computationally very costly.

6 Acknowledgements

This research was conducted as part of the AIFRI project, funded by the Federal Ministry for Digital and Transport of Germany (mFUND 19FS2014).

References

[1] DIN EN 13674-1:2017-07, railway applications - track - rail - part 1: Vignole railway rails 46 kg/m and above, 2017.

[2] Yang Bao, Praveen Gurrala, and Jiming Song. Element discretization effects on boundary element method modeling for eddy current nondestructive evaluation problems. *Journal of Nondestructive Evaluation*, 40(3):79, 2021.

[3] Alexander Friedrich. Simulation data for eddy current rail testing - simulation accuracy and evaluation uncertainty quantification, 2024.

[4] Rainer Pohl, Hans-Martin Thomas, and Ralf Casperson. Mögliche Fehlerquellen und deren Einflüsse bei der Risstiefenbestimmung mit Wirbelstrom. In *DGZfP-Jahrestagung 2009*, pages 1–11.

[5] INTEGRATED Engineering Software. Faraday, version 11.1, 2023.

[6] Noritaka Yusa, Haoyu Huang, and Kenzo Miya. Numerical evaluation of the ill-posedness of eddy current problems to size real cracks. *NDT & E International*, 40(3):185–191, 2007.

[7] Noritaka Yusa, Stephane Perrin, Kazue Mizuno, and Kenzo Miya. Numerical modeling of general cracks from the viewpoint of eddy current simulations. *NDT & E International*, 40(8):577–583, 2007.